



1 **The impact of resolving the Rossby radius at mid-latitudes**  
2 **in the ocean: results from a high-resolution version of the**  
3 **Met Office GC2 coupled model**

4 **Helene T. Hewitt<sup>1</sup>, Malcolm J. Roberts<sup>1</sup>, Pat Hyder<sup>1</sup>, Tim Graham<sup>1</sup>, Jamie Rae<sup>1</sup>,**  
5 **Stephen E. Belcher<sup>1</sup>, Romain Bourdallé-Badie<sup>4</sup>, Dan Copsey<sup>1</sup>, Andrew Coward<sup>2</sup>,**  
6 **Catherine Guiavarch<sup>1</sup>, Chris Harris<sup>1</sup>, Richard Hill<sup>1</sup>, Joël J.-M. Hirschi<sup>2</sup>, Gurvan**  
7 **Madec<sup>2,3</sup>, Matthew S. Mizieliński<sup>1</sup>, Erica Neininger<sup>1</sup>, Adrian L. New<sup>2</sup>, Jean-**  
8 **Christophe Rioual<sup>1</sup>, Bablu Sinha<sup>2</sup>, David Storkey<sup>1</sup>, Ann Shelly<sup>1</sup>, Livia Thorpe<sup>1</sup>,**  
9 **and Richard A. Wood<sup>1</sup>**

10 [1]{Met Office, Exeter, United Kingdom}

11 [2]{National Oceanography Centre, Southampton, United Kingdom}

12 [3]{IPSL, Paris, France}

13 [4]{Mercator Océan, Toulouse, France}

14 Correspondence to: H. T. Hewitt (helene.hewitt@metoffice.gov.uk)

15

16 **Abstract**

17 There is mounting evidence that resolving mesoscale eddies and boundary currents in the  
18 surface ocean field can play an important role in air-sea interaction associated with vertical  
19 and lateral transports of heat and salt. Here we describe the development of the Met Office  
20 Global Coupled Model version 2 (GC2) with increased resolution relative to the standard  
21 model: the ocean resolution is increased from 1/4° to 1/12° (28km to 9km at the Equator), the  
22 atmosphere resolution increased from 60km (N216) to 25km (N512) and the coupling  
23 frequency increased from 3-hourly to hourly. The technical developments that were required  
24 to build a version of the model at higher resolution are described as well as results from a 20  
25 year simulation. The results demonstrate the key role played by the enhanced resolution of the  
26 ocean model: reduced Sea Surface Temperature biases, improved ocean heat transports,  
27 deeper and stronger overturning circulation and a stronger Antarctic Circumpolar Current.  
28 Our results suggest that the improvements seen here require high resolution in both



1 atmosphere and ocean components as well as high frequency coupling. These results add to  
2 the body of evidence suggesting that ocean resolution is an important consideration when  
3 developing coupled models for weather and climate applications.

4

## 5 **1 Introduction**

6 On the scale of the Rossby radius, the ocean is rich with mesoscale eddies (Chelton et al.,  
7 2011) and oceanic fronts. There is mounting evidence from satellite observations that  
8 mesoscale features in the Sea Surface Temperature (SST) field can drive comparable  
9 variations in atmospheric winds and surface fluxes (Chelton and Xie, 2010; Frenger et al.,  
10 2015). While at the basin scale, observed correlations between SST and surface winds are  
11 negatively correlated, indicating that the atmosphere is driving the ocean, in frontal regions  
12 with high mesoscale activity, such as those associated with Western boundary currents, SST  
13 and surface winds are positively correlated, implying that the ocean is driving the atmosphere  
14 (Bryan et al., 2010). While the primary response to SST takes place in the atmospheric  
15 boundary layer (Chelton and Xie, 2010), there is also evidence that divergence of surface  
16 winds may give rise to vertical motions which may penetrate high into the troposphere  
17 affecting storm tracks and clouds (e.g., Minobe et al., 2008; Sheldon and Czaja, 2014). Of  
18 particular note is the intense rain band in the North Atlantic that follows the path of the Gulf  
19 Stream/North Atlantic Current.

20 The recent CMIP5 ocean models have a horizontal resolution of between  $1^\circ$  and  $1/4^\circ$ .  
21 However, with a resolution of 28km at the Equator down to 6km in the Canadian archipelago  
22 (due to the tripolar grid), even  $1/4^\circ$  remains insufficient to resolve mesoscale eddies which  
23 have a typical scale of 50km in the deep ocean at mid-latitudes (Hallberg, 2013). Several  
24 climate modelling groups have now built global coupled models with an “eddy resolving”  
25 component (e.g., McClean et al., 2011; Bryan et al., 2010; Delworth et al., 2012; Small et al.,  
26 2014; Griffies et al., 2015). In this paper, we describe results from coupling the  $1/12^\circ$  ocean  
27 model (ORCA12) produced by the Drakkar group (Marzocchi et al., 2015; Deshayes et al.,  
28 2013; Treguier et al., 2012) to a 25 km (N512) resolution version of the Met Office Unified  
29 Model (MetUM) atmosphere. This is the first version of the HadGEM3/GC series (Hewitt et  
30 al., 2011; Williams et al., 2015) to resolve the Rossby radius in the ocean at mid-latitudes  
31 (with a resolution of 9km at the Equator down to 2km in the Canadian archipelago) and the  
32 first coupled experiment with the NEMO ORCA12 ocean configuration.



1 Evidence from forced ocean simulations demonstrates that resolution enables a more realistic  
2 representation of both eddy kinetic energy (Hurlburt et al., 2009; Griffies et al., 2015), narrow  
3 boundary currents (e.g., Marzocchi et al., 2015) and representation of complex topography, in  
4 particular the sills which connect ocean basins (e.g., improved overflows in the VIKING  
5 model at 1/20° resolution; Behrens et al., 2013). In this paper we investigate how ocean  
6 resolution drives large-scale changes not only in the ocean but also in the climate system.  
7 Changes in the ocean circulation could be important both for present and future climate; for  
8 example, in an ocean-only model with a simple domain, Zhang and Vallis (2013) have shown  
9 that the changes in mean circulation due to eddy-resolving resolution can affect the net ocean  
10 heat uptake under global warming scenarios.

11 In this paper, the model is described in section 2. Our results (section 3) describe the relative  
12 impact of the three changes to the model; ocean resolution, atmosphere resolution and  
13 coupling frequency. Finally in section 4 we summarise and discuss the results.

14

## 15 **2 Model description**

16 The development of the high resolution coupled climate model is based on the Met Office  
17 Global Coupled model version 2 (GC2; Williams et al., 2015). GC2 is comprised of the Met  
18 Office Unified Model (MetUM; GA6) atmosphere, the JULES land surface model (Best et al.,  
19 2011; GL6), the NEMO ocean model (Madec, 2014; GO5; Megann et al., 2014) and the Los  
20 Alamos CICE sea-ice model (Hunke et al., 2010; GSI6; Rae et al., 2015). The standard  
21 configuration for GC2 has a 60km resolution atmosphere coupled to 1/4° (28km at the  
22 Equator reducing polewards) ocean (N216-ORCA025) with coupling between the  
23 components (as described in Hewitt et al., 2011) every three hours. GA6 has 85 vertical levels  
24 while GO5 has 75 vertical levels with 1m resolution in the top 10m of the ocean (Megann et  
25 al., 2014). Although vertical resolution is not explored here, we include details of the vertical  
26 levels in appendix A.

27 In addition to GC2, this paper describes three modified versions of GC2 with increased  
28 atmosphere resolution, increased coupling frequency and increased ocean resolution. The  
29 different model experiments are described below and summarised in Table 1.

30 GC2 has been run with a high 25km (N512) atmosphere resolution and the standard  
31 (ORCA025) resolution ocean and we will refer to this as GC2-N512. The scientific



1 differences between N216 and N512 are minimal, as described in Walters et al. (in prep), and  
2 are principally associated with the time step (modified from 15min to 10min) and the  
3 resolution of the external boundary conditions such as the orography.

4 To facilitate direct scientific comparison with the 1/12° ORCA12 (9km at the Equator  
5 reducing polewards) configuration of NEMO, which was developed using NEMO v3.5 rather  
6 than 3.4 (Marzocchi et al., 2015), a modified configuration of GC2, referred to here for  
7 convenience as GC2.1 was developed. The key scientific and technical changes made to  
8 GC2.1 are:

- 9 • an increase in the coupling frequency from 3-hourly to hourly
- 10 • an upgrade to the non-linear free surface scheme rather than the linear free surface
- 11 • a small reduction in the timestep from 1350s to 1200s (to accommodate hourly  
12 coupling)
- 13 • small changes associated with river outflows; outflows prescribed over 15m rather  
14 than 10m with an enhanced vertical mixing in the outflow region of  $1 \times 10^{-3} \text{ m}^2 \text{ s}^{-1}$  rather  
15 than  $2 \times 10^{-3} \text{ m}^2 \text{ s}^{-1}$
- 16 • an upgrade of the sea ice model from CICE4 to CICE5 (Hunke et al., 2015). This  
17 upgrade was for technical reasons and the science of the sea ice configuration remains  
18 unchanged.

19 To assess the impact of ocean resolution, a traceable GC2.1 configuration with ORCA12 was  
20 then built (further technical details and model performance issues are discussed in appendix  
21 B). We chose to increase the atmosphere resolution to N512 in order to maintain a similar  
22 aspect ratio of atmosphere to ocean grids. We will refer to this configuration as GC2.1-  
23 N512O12 (i.e., increased atmosphere and ocean resolution).

24 The differences between ORCA025 and ORCA12 in GC2.1 are:

- 25 • a reduction in the time step from 1200s to 240s
- 26 • a reduction in the isoneutral tracer diffusion from  $300 \text{ m}^2 \text{ s}^{-1}$  to  $125 \text{ m}^2 \text{ s}^{-1}$
- 27 • a reduction in the bilaplacian viscosity from  $-1.5 \times 10^{11} \text{ m}^2 \text{ s}^{-1}$  to  $-1.25 \times 10^{10} \text{ m}^2 \text{ s}^{-1}$

28 We note here that the parameter settings in GC2.1-N512O12 have not been tuned for the  
29 coupled model; the model was run using the majority of parameter settings from the forced  
30 ocean-only ORCA12 runs of Marzocchi et al. (2015).



1 GC2.1-N512O12 was found to be very sensitive to features that had not proved to be a  
2 problem in previous ocean-only integrations (e.g., Marzocchi et al., 2015). For example, the  
3 model became unstable on the east coast of the UK every 6-12 months of simulation due to  
4 extreme values in the velocity field, likely due to the lack of tides in the model which are very  
5 important in this region. The model was restarted from these failures with a small random  
6 perturbation to the atmospheric theta field in a similar way to treatment of “grid-point  
7 instabilities” previously seen in atmosphere models (e.g., Mizielinski et al 2014). The  
8 underlying problem with this unstable ocean point will be addressed in future developments  
9 of the ORCA12 configuration.

10 The GC2 and GC2.1 experiments were run for 20 years with fixed atmospheric radiative  
11 forcing representative of the present day (with greenhouse gas and aerosol values for the year  
12 2000). All experiments were initialised in the following way:

- 13 • atmosphere: N216 and N512 both from September year 18 of the model state of a  
14 previous N512 GA6 (Walters et al., in prep) forced atmosphere integration with  
15 forcing representative of the year 2000, so that the land surface properties are at quasi-  
16 equilibrium;
- 17 • ocean: temperature and salinity from the EN3 observational dataset (Ingleby and  
18 Huddleston, 2007) 2004-8 September average with velocities initialised to zero;
- 19 • sea ice: 20 year September mean from a HadGEM1 (Johns et al., 2006) experiment  
20 representative of a period centred on 1978.
- 21 • These latter two are the standard method for initialisation of “present day” coupled  
22 simulations at the Met Office.

23 The choice of the most appropriate ratio between ocean and atmosphere resolution remains an  
24 open research question worthy of further study. Short (two year) integrations using both  
25 higher and lower atmosphere resolutions coupled to ORCA12 were completed, although due  
26 to the short length of the integrations, they are not analysed here. In particular, a configuration  
27 using an N768 (17km) atmosphere led to a marked increase in the frequency of model  
28 instabilities (5-6 per year).

29



### 1 **3 Impact of model resolution on surface properties, heat transport and ocean** 2 **circulation**

3 The results shown in this section derive from 20 year simulations of the four experiments  
4 described in table 1, initialised and forced in an identical way.

5

#### 6 *a. Surface Properties*

7 The pattern of large-scale biases in SST fields in Hadley Centre coupled climate models have  
8 remained largely unchanged since the models first ran without flux correction (e.g., Gordon et  
9 al., 2000); the large-scale biases exhibit warming in the Southern Ocean, cooling in the North  
10 Pacific and North Atlantic and warming in upwelling/stratocumulus regions off the western  
11 coasts of South America and Africa. Many of these biases are also very common in other  
12 models (e.g. Small et al., 2014).

13 The time-series of the global mean Top of Atmosphere (TOA) radiation imbalance in the four  
14 models (Figure 1a) shows that the experiments with high (N512) atmosphere resolution have  
15 TOAs that are generally higher at the start of the experiments. However after 20 years all the  
16 experiments are starting to converge to a similar net TOA, as the shortwave and long-wave  
17 components adjust. Although the TOA-SST relationship is poorly defined (since the TOA  
18 imbalance is related to the rate of change of net ocean heat content; Palmer and McNeill,  
19 2014), the integrated effect of the higher net TOA in the N512 experiments can be seen in the  
20 timeseries of the global mean SST (Figure 1b) with GC2-N512 and GC2.1-N512O12 having  
21 higher global mean SSTs.

22 In spite of the differences in global mean SST, major changes to the pattern and magnitude of  
23 SST biases are only seen with both high atmosphere and ocean resolution (Figure 2). In  
24 GC2.1 N512-ORCA12, the large-scale underlying SST biases are reduced relative to GC2 and  
25 GC2.1 (Figure 3): the warm bias in the Southern Ocean; cold bias in North Atlantic and North  
26 Pacific and warm biases in stratocumulus regions. Similar reductions in SST biases with high  
27 atmosphere and ocean resolution were also seen in Small et al. (2015). The increase in ocean  
28 resolution is key to this improvement: when only atmosphere resolution is increased (compare  
29 Figures 2a and b), there is only a small reduction in the warm bias associated with  
30 stratocumulus regions (west of South America and Africa), while increased coupling  
31 frequency (compare Figures 2a and c) shows only minor changes in SST biases.



1 In GC2 there is a cold bias in the North Atlantic subpolar gyre (SPG), Greenland-Iceland-  
2 Norwegian (GIN) Seas and the Arctic. GC2.1-N512O12 shows a warming of several degrees  
3 in the SPG and GIN seas relative to GC2 (see reduced cold bias in Figure 2d) and a very large  
4 warming in the Central Arctic. The warming in the Central Arctic is associated with a  
5 warming in the subpolar gyre, enhanced northward heat transport into the Arctic and melting  
6 back of the sea ice edge in the Arctic (see below).

7 Resolution appears to have less of an impact on Sea Surface Salinity (SSS; Figure 4).  
8 Nevertheless, there are reductions in high salinity biases in the Indian Ocean and the Pacific  
9 (in particular, in the salinity maximum in the subtropical gyre of the South Pacific) as well as  
10 reductions in the Arctic biases (although these are very sensitive to the distribution of sea ice).

11

#### 12 *b. Sea ice*

13 The changes to the SST also affect sea ice distribution in both hemispheres. The seasonal  
14 cycle of ice extent in the Arctic (Figure 5a) shows that the warm SSTs in GC2.1-N512O12 at  
15 high Northern latitudes reduce the ice extent throughout the year. The March ice  
16 concentrations in the Arctic (Figure 6) clearly demonstrate that the impact on the sea ice is  
17 concentrated in the GIN seas with the sea ice edge in GC2.1-N512O12 much further north  
18 than seen in GC2 with the edge being north of Spitzbergen and into the Barents Sea.

19 In comparison, the reduction in the warm bias in the Southern hemisphere leads to only  
20 modest increases in the total sea ice extent (Figure 5b); the overall warming bias associated  
21 with the lack of super-cooled liquid clouds (Bodas-Salcedo et al., 2014; Bodas-Salcedo et al.,  
22 in press) still dominates the melting of sea ice. The small increase in sea ice extent is very  
23 inhomogeneous; indeed, some regions in the Southern Ocean such as the Weddell Sea  
24 actually show reductions in sea ice extent in GC2.1 N512-ORCA12 (Figure 6). The reduction  
25 in the Weddell Sea is associated with a polynya in that region (see below).

26

#### 27 *c. Sub-surface ocean drifts*

28 Conservation of heat within the climate system implies that the net heat uptake by the ocean  
29 should nearly balance the net radiative imbalance at the TOA. GC2.1-N512O12 has the  
30 highest TOA imbalance of the four models (Table 2) and therefore will have the greatest net  
31 heat uptake. Both models with increased atmosphere resolution (GC2-N512 and GC2.1-



1 N512O12) have a higher TOA imbalance than the models with lower atmosphere resolution  
2 (GC2 and GC2.1).

3 The global temperature profiles (Figure 7a) show that GC2-N512 and GC2.1-N512O12 do  
4 indeed have greater increases in temperature as a function of depth than either of the low  
5 resolution models (GC2 and GC2.1), which is consistent with the higher TOA imbalance. The  
6 main difference between GC2-N512 and GC2.1-N512O12 is that the increase in heat uptake  
7 extends deeper in GC2.1-N512O12. This difference is also apparent in the global mean SST  
8 anomaly (Table 2); the SST anomaly for years 11-20 in GC2.1-N512O12 is 0.44 K compared  
9 with 0.60 K in GC2-N512, while the TOA imbalance is 2.02 W/m<sup>2</sup> and 1.79 W/m<sup>2</sup>  
10 respectively. This shows that the ORCA12 version of the model is able to transport heat to  
11 depth more effectively.

12 The distribution of the subsurface temperature changes varies depending on the latitudinal  
13 range. South of 30°S (Figure 7b), near surface warming is reduced in GC2.1-N512O12  
14 relative to the other models. In the Tropics (30°S-30°N; Figure 7c), GC2.1-N512O12 shows  
15 increased warming shallower than 500m relative to the low resolution models but reduced  
16 relative to GC2-N512. The Tropics also show increased warming at depth in GC2.1-  
17 N512O12. The largest increase in near surface temperatures in GC2.1-N512O12 relative to  
18 the other models occurs north of 30°N (Figure 7d) with the surface warming displacing a cold  
19 bias to deeper in the water column. The warming is particularly concentrated north of 65°N  
20 (Figure 7e) where it has previously been shown that Arctic sea ice melts back.

21 Drifts in sub-surface salinity show that GC2.1-N512O12 generally has larger salinity drifts  
22 between 500 and 1000m (Figure 8a) which is largely associated with the region south of 30°S  
23 (Figure 8b). In the northern hemisphere, drifts in salinity between 1000 and 2000m are also  
24 more pronounced in GC2.1-N512O12 than the other models (Figure 8d). In contrast, large  
25 fresh biases north of 65°N in most of the models is much reduced in GC2.1-N512O12 (Figure  
26 8e). Understanding salinity drifts and their relationship to freshwater forcing is complex (eg,  
27 Pardaens et al. 2003) and this aspect of the model performance will require further  
28 investigation.

29

30

31





1        *d. Mixed layer depths*

2        In general over the open oceans, the mixed layer depths (Figure 6) are very similar across the  
3        different models and it is in the deep water formation regions where we see inter-hemispheric  
4        changes. Winter mixed layers in the Northern hemispheres in GC2.1-N512O12 show a  
5        reduction in the North Atlantic subpolar gyre. Most notably, in GC2.1-N512O12 deep mixed  
6        layers are less extensive south of Greenland than in GC2 and are confined to the centre of the  
7        Labrador Sea. Similar changes in Labrador Sea deep convection have been seen in sensitivity  
8        experiments when overflow properties are improved (Graham et al., in prep.). The deeper  
9        mixed layers in the Arctic in GC2.1-N512O12 are consistent with warmer SSTs and reduced  
10       sea ice extent in that region exposing open water.

11       The similarity of the mixed layer depths across the Southern Ocean demonstrate that it is not  
12       changes to the mixed layer depths that lead to a reduction in the Southern Ocean warm bias.  
13       As mentioned in the previous section, in the Weddell Sea, GC2.1-N512O12 has very deep  
14       mixed layers linked to a polynya, which explains the lack of increase of sea ice extent in that  
15       region (Figure 6). Deeper winter mixed layers in GC2.1-N512O12 are also evident through  
16       the mid-latitudes in the formation zones for Sub-Antarctic Mode Waters and Antarctic  
17       Intermediate Waters. These could be due to the reduced warm bias (cooler SSTs) in these  
18       regions (Figure 2).

19

20       *e. Ocean Circulation*

21       The improvements seen in the large-scale SST biases with high atmosphere and ocean  
22       resolution (Figure 3) represent an overall improvement in the model simulation with warming  
23       in the Northern hemisphere and cooling in the Southern hemisphere. This pattern is  
24       reminiscent of inter-hemispheric modes that occur as a result of changes in the large-scale  
25       thermohaline circulation (Vellinga and Wu, 2004). The meridional overturning in our  
26       simulations changes only in the GC2.1-N512O12, with an increase of O(3 Sv) (Table 2) both  
27       in the North and South Atlantic, and is therefore attributed to the increased ocean resolution.  
28       The changes in the meridional overturning circulation (Figure 9) are dominated by changes in  
29       the cell associated with North Atlantic Deep Water (NADW) with changes extending into the  
30       Southern hemisphere.



1 At the northern end of the NADW cell, we see increases in the volume flux of dense  
2 overflows between the GIN Seas and the Atlantic (Table 2) that are consistent with the  
3 NADW cell being strengthened both by the GIN sea sources and better representation of sills.  
4 The volume flux of overflow waters across Denmark Straits generally reduces fairly rapidly  
5 in ORCA025 runs (Figure 10a) but in GC2.1-N512O12 the overflow remains closer to the  
6 observed value of 2.9 - 3.7 Sv (Dickson and Brown, 1994; Macrander et al., 2005). This  
7 appears to also contribute to a deeper (as well as stronger) NADW outflow in this model and  
8 is almost certainly associated with the increased resolution of the topography in the region of  
9 the overflows.

10 The Antarctic Circumpolar Current (ACC) usually drifts in the ORCA025 GC models from  
11 an initial value of approximately 150 Sv to below 100 Sv (Figure 10b). Increased ocean  
12 resolution counteracts that, with the ACC stabilising close to 130 Sv in this 20 year  
13 experiment. This value is close to the observations that suggest an ACC transport of  $137 \pm 8$   
14 Sv (Cunningham et al., 2003)). The increase in the transport in the ACC can be explained by  
15 changes in the density field; the meridional density gradients across the ACC (not shown) are  
16 increased in GC2.1-N512O12 (with steeper isopycnals) than in GC2 which is consistent with  
17 increased southward flow, and stronger upwelling, of NADW to the north of the ACC and  
18 increased convection to the south of the ACC in the Weddell Sea. The Southern Ocean winds  
19 (not shown) respond differently across the four simulations (including a small increase in  
20 GC2.1-N512O12 and a decrease in GC2.1) and investigating these changes, how they relate  
21 to the model internal variability and their impact on the simulation will be a topic of future  
22 research.

23

#### 24 *f. Heat transport*

25 As described in Gordon et al. (2000), drifts in volume averaged ocean temperature can be  
26 related to discrepancies between the actual heat transports by the ocean and the heat transport  
27 implied by the surface fluxes, i.e.

$$28 \quad \frac{\partial \rho c_p \langle \theta \rangle}{\partial t} + \oint \rho c_p (\bar{v} \bar{\theta} + \overline{v' \theta'}) dS + \oint \rho c_p A_{iso} \nabla_{\rho} \theta dS = \int F dA, \quad (1)$$

29 where  $\langle \theta \rangle$  is the volume integrated temperature,  $\bar{v} \bar{\theta}$  and  $\overline{v' \theta'}$  are the time mean and time  
30 varying components of the ocean meridional heat transports,  $\rho c_p$  is density multiplied by  
31 specific heat capacity,  $A_{iso}$  is the isopycnal diffusion,  $\nabla_{\rho} \theta$  is the isoneutral gradients of



1 temperature and  $F$  is the surface heat flux. For our purposes here, we make the assumption  
2 that the isoneutral fluxes are generally smaller than the other terms (dianeutral diffusive  
3 fluxes are very small when integrated over full depth).

4 Figure 11a shows the global northward heat transport in all four simulations. There are some  
5 changes in the northern hemisphere in the GC2.1 simulation with the change to hourly  
6 coupling, while changes in the southern hemisphere are only seen in GC2.1-N512O12  
7 suggesting that these changes are driven by the increase in ocean resolution. The reduction in  
8 southward heat transport in GC2.1-N512O12 centred at 45°S is highly unusual; although the  
9 change does not lie outside interannual variability, a change of this magnitude in the multi-  
10 year mean heat transport has not been seen in any other development runs of the GC series.  
11 The modelled changes in the heat transports suggest that ocean processes are important in this  
12 region, which is particularly relevant given the uncertainty in surface heat fluxes in the  
13 Southern Ocean (Cerovecki et al., 2011). The change in total heat transport comes primarily  
14 from the time mean heat transport (not shown). This suggests that changes in resolution have  
15 led to a change in either the mean circulation or the temperature profile (as opposed to a  
16 change in the time varying heat transport, which would imply a direct role of the mesoscale  
17 eddies). As seen in previous sections, GC2.1-N512O12 shows changes in both the circulation  
18 and the temperature profiles. The decreased southward heat transport in the Southern Ocean  
19 of GC2.1-N512O12 could – at least partly - explain the reduced warm bias.

20 By comparing actual ocean heat transports with those implied by surface fluxes (i.e., the  
21 second term of the left-hand side of Eqn. 1 with the right-hand side of Eqn. 1), this gives an  
22 indication of the volume averaged drift in temperature (first term on the left-hand side of Eqn.  
23 1). The implied ocean heat transport is calculated by subtracting the globally averaged  
24 imbalance from the surface fluxes before integrating zonally and meridionally. Globally  
25 (Figure 11a) GC2.1-N512O12 can be seen to be as close to local balance as any of the other  
26 models, suggesting that the net drifts will be of a similar magnitude (in agreement with Figure  
27 5).

28 Ocean resolution is the driving factor in a 0.2PW increase in the northward heat transport in  
29 the Atlantic; the modelled heat transports in GC2.1-N512O12 are generally within the error  
30 bars of the observations (Ganachaud and Wunsch, 2003; Figure 11b) in contrast to the other  
31 models with the lower resolution ocean component. The change in heat transport is linked to  
32 an increase in the overturning circulation (previous section), which is unsurprising given the



1 dominant role of the meridional overturning circulation in the Atlantic heat transport (Hall  
2 and Bryden, 1982).

3

#### 4 **4 Summary and Discussion**

5 In this paper we have shown results from a coupled climate model with an eddy resolving  
6 ( $1/12^\circ$ ) ocean component coupled to a high resolution (25 km) atmosphere component. When  
7 the SST bias from this climate simulation is compared to that from the Met Office standard  
8 resolution climate model, with eddy permitting ( $1/4^\circ$ ) ocean component and 60km atmosphere  
9 component, it is apparent that major SST biases in the Southern Ocean and North Atlantic and  
10 North Pacific have been reduced. Comparable experiments increasing only the atmosphere  
11 resolution or the coupling frequency, demonstrate that increased ocean resolution is the key  
12 driver for this change.

13 At the enhanced ocean resolution, the ocean circulation leads to increased poleward ocean  
14 heat transport in the Northern hemisphere and reduced poleward ocean heat transport in the  
15 Southern hemisphere. The change in the northward heat transport is driven at least in part by  
16 an enhanced NADW cell which also contributes to maintaining the ACC front. The ACC  
17 front is maintained in spite of the expectation that improved representation of eddies in the  
18 Southern Ocean could lead to slumping of the front, this is at least in part associated with  
19 enhanced windstresses at high resolution. Changes in the global heat transports produce a  
20 shift in the large-scale biases, cooling the Southern Ocean and warming the North Atlantic  
21 and North Pacific. We have shown that heat penetrates deeper in our  $1/12^\circ$  model; Griffies et  
22 al. (2015) have demonstrated that mesoscale eddies transport heat upwards so it is likely that  
23 the increased transport of heat to depth is achieved by the time-mean as seen in transient  
24 experiments such as Banks and Gregory (2006). Future work will be focused on  
25 understanding the relative roles of resolving overflow topography (Behrens, 2013), eddy  
26 processes within the ocean including compensation and saturation (e.g., Munday et al., 2013)  
27 and air-sea interaction on the eddy scale (Roberts et al., in prep.) in driving the large-scale  
28 changes.

29 Relative to the recent high resolution results of Small et al. (2014) and Griffies et al. (2015),  
30 our results emphasise the importance of increasing both atmosphere and ocean resolution.  
31 Griffies et al. (2015) show smaller reductions in SST biases when moving from  $1/4^\circ$  to  $1/10^\circ$   
32 resolution presumably related to keeping the atmosphere resolution unchanged. Enhanced



1 coupling frequency along with enhanced vertical resolution near the air-sea interface both in  
2 the ocean (Megann et al., 2014) and atmosphere (Walters et al., in prep) is one feature of our  
3 model setup that is missing in Small et al. (2014). These aspects of the model setup may be  
4 especially important in regions of strong air-sea interaction including the stratocumulus  
5 regions where we see large improvements in the GC2.1-N512O12 simulation. Overall, the  
6 improvements seen in this paper required a combination of high resolution in both atmosphere  
7 and ocean components as well as high frequency coupling.

8 As described in the previous section, one of the changes to the ocean model at higher  
9 resolution was a reduction in the isoneutral diffusion. Pradal and Gnanadesikan (2014) show  
10 that a reduction in the isoneutral diffusion from  $800 \text{ m}^2\text{s}^{-1}$  to  $400 \text{ m}^2\text{s}^{-1}$  in a coarse resolution  
11 climate model is associated with cooling of order  $1^\circ\text{C}$  at high latitudes after 500 years. While  
12 the results here may exhibit some consistency with those of Pradal and Gnanadesikan (2014)  
13 in the Southern Ocean, the change in isopycnal diffusion is believed to be a secondary effect  
14 due to the fact that we are seeing a comparable or larger change in SST in a short 20 year run.

15 One caveat of these results is that the parallel simulations lasted only 20 years. However, the  
16 close agreement between implied and actual meridional heat transports, suggests that the  
17 models are close to quasi-equilibrium. Additionally, the broad similarity of the results  
18 presented here compared with those of Small et al. (2014) from over 100 years of simulation  
19 suggest that the results are reasonably robust. In terms of model drift, climate models  
20 typically have a fast adjustment within the first five years (Sanchez-Gomez et al., 2016).  
21 Large adjustments over the first 20 years are generally followed by a multi-centennial drift  
22 towards equilibrium between ocean properties and the net TOA flux (Banks et al., 2007).  
23 Longer simulations and further analyses will enable the robustness of the results presented  
24 here (including wind-SST feedbacks) to be more fully understood.

25 In the results here, the  $1/12^\circ$  ocean model, which has a resolution of approximately 7 km at  
26 mid-latitudes, is coupled to an N512 atmosphere model, which has a resolution of 25 km. An  
27 atmosphere:ocean ratio of 4:1 may be too high for the atmosphere to fully capture the details  
28 of the ocean mesoscale. Future work will investigate the impact of coupling to even higher  
29 resolution atmosphere models to investigate the role of the atmosphere:ocean ratio.

30 As we move towards seamless coupled prediction, using coupled models for prediction on  
31 timescales from days to centuries, the results presented here are highly relevant to prediction  
32 up to decadal timescales where data assimilation is employed. A coupled model that more



1 faithfully produces the current state of the ocean will rely less on data assimilation for  
2 correcting large-scale biases and be more able to include the representation of spatial  
3 anomalies that control the large-scale variability. While there are many regions where  
4 subsurface drifts are improved at this resolution, reducing the drifts seen in mid-depth salinity  
5 will be important.

6 A key question for these timescales is whether employing enhanced resolution will address  
7 the known problem of low signal-to-noise ratios (Eade et al., 2014) that has led to the need for  
8 large ensembles for seasonal to decadal forecasting in lower resolution systems. Future work  
9 to understand the drivers of large-scale bias reduction will support targeted experiments to  
10 address the relative roles of resolution and ensemble size at these timescales. That said, ocean  
11 resolution is clearly not going to solve all the issues in climate models; atmosphere errors  
12 often dominate surface biases and, even at high resolution, ocean models need improved  
13 representation of sub-gridscale processes.

14  
15

#### 16 **Code availability**

17 The MetUM is available for use under licence. A number of research organizations and  
18 national meteorological services use the MetUM in collaboration with the Met Office to  
19 undertake basic atmospheric process research, produce forecasts, develop the MetUM code  
20 and build and evaluate Earth system models. For further information on how to apply for a  
21 licence see <http://www.metoffice.gov.uk/research/collaboration/um-collaboration>. JULES is  
22 available under licence free of charge. For further information on how to gain permission to  
23 use JULES for research purposes see <https://jules.jchmr.org/software-and-documentation>. The  
24 model code for NEMO v3.4 and v3.5 is available from the NEMO website ([www.nemo-](http://www.nemo-ocean.eu)  
25 [ocean.eu](http://www.nemo-ocean.eu)). On registering, individuals can access the code using the open source subversion  
26 software (<http://subversion.apache.org/>). The model code for CICE is freely available  
27 (<http://oceans11.lanl.gov/trac/CICE/wiki/SourceCode>) from the United States Los Alamos  
28 National Laboratory. In order to implement the scientific configuration of GC2/GC2.1 and to  
29 allow the components to work together, a number of branches (code changes) are applied to  
30 the above codes. Please contact the authors for more information on these branches and how  
31 to obtain them.



1 **Appendix A: Model vertical levels**

2 The sensitivity to vertical resolution is not explored in this paper. However, a reduced  
3 description of the vertical levels in GA6 (Table A1) and GO5 (Table A2) are included to  
4 allow comparison with other models. For the full vertical levels, see Walters et al. (in prep.)  
5 and Megann et al. (2014), respectively.

6

7

Level	Rho_height (m)
1	10.00
10	730.00
20	2796.67
30	6196.67
40	10930.12
50	17012.40
60	24710.70
70	35927.89
80	58978.35
85	82050.01

8 Table A1: Reduced list of level in GA6 which has 85 vertical levels

9



1

Level	Depth (m)	Thickness (m)
1	0.51	1.02
10	13.99	2.37
20	61.11	7.58
30	180.55	18.27
40	508.64	53.76
50	1387.38	125.29
60	2955.57	181.33
65	3897.98	194.29
70	4888.07	200.97
75	5902.06	204.23

2 Table A2: Reduced list of levels and layer thicknesses in GO5 which has 75 vertical levels

3





## 1 **Appendix B: Model performance and technical aspects**

2 The GC2.1 configuration was the first in which several further technical components of the  
3 coupled system were considered essential to make the simulation manageable. The coupler  
4 was upgraded from OASIS3 to OASIS3-MCT (Valcke et al, 2015) in order to improve  
5 parallelisation of the coupling, particularly given the increased coupling frequency.

6 ORCA025 files are typically written as one file per processor by standard GC2 configurations  
7 and combined into a single file prior to analysis as a post processing step. However, as HPC  
8 parallel file systems are generally tuned for high bandwidth on large files and as GC2.1-  
9 N512O12 configurations allocate 50 of the 80 nodes used by the full coupled system to the  
10 ocean, this led to performance and functional issues when running on 1600 or more cores.  
11 The NEMO XIOS diagnostic server (Madec, 2014) provides an asynchronous IO server  
12 capability that allows the diagnostic files to be output as fewer larger files (although the  
13 restart files are still written as one file per processor). Its introduction in the model allowed us  
14 to overcome the limitations of the file system.

15 Land suppression was used for the NEMO and CICE models, so that processors are only  
16 assigned to regions with active ocean points. This leads to a significant gain in core count,  
17 although it meant that the automated large-scale diagnostics usually produced by NEMO  
18 (zonal mean heat transports, meridional overturning) could not be generated.

19 Data volumes from this experiment were particularly large due to the output of additional  
20 hourly and 3-hourly fluxes in order to examine the coupling processes in more detail. Each  
21 month of model output comprised: ocean monthly mean files (netCDF) of 87GB together  
22 with 6GB of daily files, sea-ice output (netCDF) of 57GB per month (with an additional  
23 48GB of hourly output), and atmosphere output (PP format) of 100 GB per month. In total,  
24 the 20 years of simulation produced 85 TB of data.

25 Little optimisation of the model was attempted since GC2.1 is not intended to be supported in  
26 the long-term. Its successor, GC3, will be used for CMIP6. The GC2.1-N512O12 model used  
27 80 full nodes (each of 32 cores) of an IBM Power 7 HPC, of which 55 were allocated to the  
28 ocean/sea ice component (including 5 for the IO servers) and 25 for the atmosphere/land  
29 component. The model throughput was 4 months per wall-clock day.

30 For previous model resolutions, the SCRIP utility (Jones, 1998) was used to generate the  
31 conservative remapping files used to regrid coupling data between the ocean and atmosphere



1 grids (for temperature and fluxes), with bilinear interpolation used for the winds and surface  
2 currents. However, due to the size of the high resolution grids used here, and the serial nature  
3 of SCRIP, a different method was required. ESMF (ESMF, 2014; a package of parallelised  
4 tools that use the same input grid descriptions as SCRIP, but can be run in parallel) was  
5 therefore used to generate the remapping weights.

6

7

## 8 **Acknowledgements**

9 This work was primarily supported by the Joint DECC/Defra Met Office Hadley Centre  
10 Climate Programme (GA01101). Part of the work was undertaken with National Capability  
11 funding from NERC for ocean modelling. We acknowledge use of the MONSooN system, a  
12 collaborative facility supplied under the Met Office-NERC Joint Weather and Climate  
13 Research Programme (JWCRP). Met Office authors were supported by the joint UK  
14 DECC/DEFRA Met Office Hadley Centre Climate Programme (GA01101). MR  
15 acknowledges support from the EU FP7 IS-ENES2 project for work on ESMF and regridding  
16 tools. We acknowledge the considerable effort on development and evaluation of ORCA12 by  
17 the DRAKKAR community. HH thanks IH.

18

19

## 20 **References**

21 Banks, H. T. and Gregory, J. M.: Mechanisms of ocean heat uptake in a coupled climate  
22 model and the implications for tracer based predictions of ocean heat uptake, *Geophys. Res.*  
23 *Let.*, 33, L076208, doi:10.1029/2005GL025352, 2006.

24 Banks, H. T., Stark, S. and Keen, A. B.: The adjustment of the coupled climate model  
25 HadGEM1 towards equilibrium and the impact on global climate, *J. Climate*, 20, 5815-5826,  
26 2007.

27 Behrens, E.: The oceanic response to Greenland melting: the effect of increasing model  
28 resolution, PhD thesis, University of Kiel, 2013.

29 Best, M. J., Pryor, M., Clark, D. B., Rooney, G. G., Essery, R. L. H., Ménard, C. B., Edwards,  
30 J. M., Hendry, M. A., Porson, A., Gedney, N., Mercado, L. M., Sitch, S., Blyth, E., Boucher,



- 1 O., Cox, P. M., Grimmond, C. S. B., and Harding, R. J.: The Joint UK Land Environment  
2 Simulator (JULES), model description – Part 1: Energy and water fluxes, *Geosci. Model*  
3 *Dev.*, 4, 677–699, doi:10.5194/gmd-4-677-2011, 2011
- 4 Bodas-Salcedo, A., Williams, K. D., Ringer, M. A., Beau, I., Cole, J. N. S., Dufresne, J.-L.,  
5 Koshiro, T., Stevens, B., Wang, Z. and Yokohata, T.: Origins of the solar radiation biases  
6 over the Southern Ocean in CFMIP2 models, *J. Climate*, 27, 41-56, doi:10.1175/JCLI-D-13-  
7 00169.1., 2014.
- 8 Bodas-Salcedo, A., Hill, P. G., Furtado, K., Karmalkar, A., Williams, K. D., Field, P. R.,  
9 Manners, J. C., Hyder, P. and Kato, S.: Large contribution of supercooled liquid clouds to the  
10 solar radiation budget of the Southern Ocean, *J. Climate*, in press.
- 11 Bryan, F. O., Tomas, R., Dennis, J. M., Chelton, D. B., Loeb N. G. and McClean J. L.:  
12 Frontal scale air-sea interaction in high-resolution coupled climate models, *J. Clim.*,  
13 doi:10.1175/2010JCLI3665.1, 2010.
- 14 Cerovecki, I., Talley, L. D., Mazloff, M. R.: A Comparison of Southern Ocean Air-Sea  
15 Buoyancy Flux from an Ocean State Estimate with Five Other Products. *Journal of Climate*.  
16 24:6283-6306, 2011.
- 17 Chelton, D. B. and Xie, S.-P.: Coupled ocean-atmosphere interaction at oceanic mesoscales,  
18 *Oceanography*, 23(4), 52-69, 2010.
- 19 Chelton, D. B., Schlax, M. G. and Samelson, R. M.: Global observations of nonlinear  
20 mesoscale eddies, *Prog. Oceanogr.*, 91, 167-216, 2011.
- 21 Cunningham, S. A., Alderson, S. G., King, B. A. and Brandon, M. A.: Transport and  
22 variability of the Antarctic Circumpolar Current in Drake Passage, *J. Geophys. Res.*, 108,  
23 doi:10.1029/2001JC001147, 2003.
- 24 Delworth, T. L., Rosati, A., Anderson, W. G., Adcroft, A., Balaji, V., Benson, R., Dixon, K.  
25 W., Griffies, S. M., Lee, H.-C., Pacanowski, R. C., Vecchi, G. A., Wittenberg, A. T., Zeng,  
26 F., and Zhang, R.: Simulated climate and climate change in the GFDL CM2.5 high-resolution  
27 coupled climate model. *Journal of Climate*, 25(8), doi:10.1175/JCLI-D-11-00316.1, 2012.
- 28 Deshayes, J., Treguier, A. -M., Barnier, B., Lecomte, A., Le Sommer, J, Molines, J.-M.,  
29 Penduff, T., Bourdalle-Badie, R., Drillet, Y., Garric, G., Benshila, R., Madec, G., Biastoch,  
30 A., Boening, C. W., Scheinert, M., Coward, A. C. and Hirschi, J. J.: Oceanic hindcast



- 1 simulations at high resolution suggest that the Atlantic MOC is bistable, *Geophys. Res. Lett.*,  
2 40, 3069-3073 doi:10.1002/grl.50534, 2013.
- 3 Dickson R.R., Brown J.: The production of North Atlantic Deep Water: Sources, rates, and  
4 pathways. *J Geophys Res* 99(C6):12,319–12,341, DOI 10.1029/94jc00530, 1994.
- 5 Eade, R., Smith D., Scaife A., Wallace E., Dunstone N., Hermanson L. and Robinson N.: Do  
6 seasonal to decadal predictions underestimate the predictability of the real world?, *GRL*, DOI:  
7 10.1002/2014GL061146, 2014.
- 8 ESMF: Earth System Modelling Framework Reference Manual for Fortran, 2014. Available  
9 from  
10 [http://www.earthsystemmodeling.org/esmf\\_releases/public/ESMF\\_6\\_3\\_Orp1/ESMF\\_refdoc](http://www.earthsystemmodeling.org/esmf_releases/public/ESMF_6_3_Orp1/ESMF_refdoc)
- 11 Frenger, I., Gruber, N., Knutti, R. and Munnich, M.: Imprint of Southern Ocean eddies on  
12 winds, clouds and rainfall, *Nature Geoscience*, 6, 608-612, 2013.
- 13 Ganachaud, A. and Wunsch, C.: Large-scale ocean heat and freshwater transports during  
14 World Ocean Circulation Experiment, *J. Climate*, 16, 696-705, 2003.
- 15 Gordon C., Cooper, C., Senior, C. A., Banks, H., Gregory, J. M., Johns, T. C., Mitchell, J.  
16 F. B., and Wood, R. A.: The simulation of SST, sea ice extents and ocean heat transports in a  
17 version of the Hadley Centre coupled model without flux adjustments, *Climate Dynamics*, 16,  
18 147-168, 2000.
- 19 Griffies, S. M., Winton, M., Anderson, W. G., Benson, R., Delworth, T. L., Dufour, C. O.,  
20 Dunne, J. P., Goddard, P., Morrison, A. K., Rosati, A., Wittenberg, A. T., Yin, J. J. and  
21 Zhang, R.: Impacts on Ocean Heat from Transient Mesoscale Eddies in a Hierarchy of  
22 Climate Models, *J. Climate*, 28, 952-977, 2015.
- 23 Hall, M. M., and Bryden, H. L.: Direct estimates and mechanisms of ocean heat transport,”  
24 *Deep-Sea Res.*, **29**, No. 3A, 339–359, 1982.
- 25 Hallberg, R.: Using a Resolution Function to Regulate Parameterizations of Oceanic  
26 Mesoscale Eddy Effects. *Ocean Modelling*, 72, DOI:10.1016/j.ocemod.2013.08.007, 2013.
- 27 Hewitt, H. T., Copsey, D., Culverwell, I. D., Harris, C. M., Hill, R. S. R., Keen, A. B.,  
28 McLaren, A. J. and Hunke, E. C.: Design and implementation of the infrastructure of  
29 HadGEM3: the next-generation Met Office climate modelling system, *Geosci. Model Dev.*, 4,  
30 223-253, doi:10.5194/gmd-4-223-2011, 2011.



- 1 Hunke, E. C. and Lipscomb, W. H.: CICE: the Los Alamos sea ice model documentation and  
2 software users' manual, Version 4.1, LA-CC-06-012, Los Alamos National Laboratory, N.M.,  
3 2010.
- 4 Hunke, E. C., Lipscomb, W. H., Turner, A. K., Jeffery, N. and Elliott, S.: CICE: The Los  
5 Alamos Sea Ice Model, Documentation and Software User's Manual, Version 5.1. Tech. Rep.  
6 LA-CC-06-012, Los Alamos National Laboratory, Los Alamos, New Mexico. Available  
7 from: <http://oceans11.lanl.gov/trac/CICE>, 2015.
- 8 Hurlburt, H. E., Brassington, G. B., Drillet, Y., Kamachi, M., Benkiran, M., Bourdalle-Badie,  
9 R., Chassignet, E. P., Jacobs, G. A., Le Galloudec, O., Lellouche, J. M., Metzger, E. J.,  
10 Smedstad, O. M., and Wallcraft, A. J.: High-Resolution Global and Basin-Scale Ocean  
11 Analyses and Forecasts, *Oceanography*, 22(3), 110-127, 2009.
- 12 Ingleby, B. and Huddleston, M.: Quality control of ocean temperature and salinity profiles -  
13 Historical and real-time data. *J. Mar. Sys.*, 65, 158-175, 2007.
- 14 Jones P. W.: A User's Guide for SCRIP: A Spherical Remapping and Interpolation Package,  
15 Version 1.5, Los Alamos National Laboratory, 1998.
- 16 Johns, T. C., Durman, C. F., Banks, H. T., Roberts, M. J., McLaren, A. J., Ridley, J. K.,  
17 Senior, C. A., Williams, K. D., Jones, A., Rickard, G. J., Cusack, S., Ingram, W. J., Crucifix,  
18 M., Sexton, D. M. H., Joshi, M. M., Dong, B. W., Spencer, H., Hill, R. S. R., Gregory, J. M.,  
19 Keen, A. B., Pardaens, A. K., Lowe, J. A., Boda-Saloedo, A., Stark, S. and Searl, Y.: The new  
20 Hadley Centre climate model HadGEM1: Evaluation of coupled simulations in comparison to  
21 previous models, *J. Climate*, 19 (7), 1327–1353 , 2006.
- 22 McClean, J. L., Bader, D. C., Bryan, F. O., Maltrud, M. E., Dennis, J. M., Mirin, A. A., Jones,  
23 P. W., Kim, Y. Y., Ivanova, D. P., Vertenstein, M., Boyle, J. S., Jacob, R. L., Norton, N.,  
24 Craig, A. and Worley, P. H.: A prototype two-decade fully-coupled fine-resolution CCSM  
25 simulation. *Ocean Modelling*. 39:10-30. 10.1016/j.ocemod.2011.02.011, 2011.
- 26 Macrander, A., Send, U., Valdimarsson, H., Jonsson, S. and Kase, R. H.: Interannual changes  
27 in the overflow from the Nordic Seas into the Atlantic Ocean through Denmark Strait.  
28 *Geophys Res Lett* 32(6):L06,606+, DOI 10.1029/2004gl021463, 2005.
- 29 Madec, G.: "NEMO ocean engine". Note du Pôle de modélisation, Institut Pierre-Simon  
30 Laplace (IPSL), France, No 27 ISSN No 1288-1619, 2014.



- 1 Marzocchi, A., Hirschi, J. J. M., Holliday, N. P., Cunningham, S. A., Blaker, A. T. and  
2 Coward, A. C.: The North Atlantic subpolar circulation in an eddy-resolving global ocean  
3 model. *Journal of Marine Systems*, 142, 126-143. 10.1016/j.jmarsys.2014.10.007, 2015.
- 4 Megann, A.P., Storkey, D., Aksenov, Y., Alderson, S., Calvert, D., Graham, T., Hyder, P.,  
5 Siddorn, J. and Sinha, B.: GO 5.0: The joint NERC-Met Office NEMO global ocean model  
6 for use in coupled and forced applications. *Geosci. Model Dev.*, 7 (3). 1069-1092.  
7 10.5194/gmd-7-1069-2014, 2014.
- 8 Minobe, S., Kuwano-Yoshida, A., Komori, N., Xie, S.-P. and Small, R. J.: Influence of the  
9 Gulf Stream on the troposphere, *Nature*, 452, doi:10.1038/nature06690, 2008.
- 10 Mizieliński, M. S., Roberts, M. J., Vidale, P. L., Schiemann, R., Demory, M.-E., Strachan, J.,  
11 Edwards, T., Stephens, A., Lawrence, B. N., Pritchard, M., Chiu, P., Iwi, A., Churchill, J., del  
12 Cano Novales, C., Kettleborough, J., Roseblade, W., Selwood, P., Foster, M., Glover, M., and  
13 Malcolm, A.: High-resolution global climate modelling: the UPSCALE project, a large-  
14 simulation campaign, *Geosci. Model Dev.*, 7, 1629-1640, doi:10.5194/gmd-7-1629-2014,  
15 2014.
- 16 Munday, D. R., Johnson, H. L. and Marshall, D. P.: Eddy saturation of equilibrated  
17 circumpolar currents, *J. Phys. Oceanogr.*, 43, 507-532, 2013.
- 18 Palmer, M. D., and McNeall, D. J.: Internal variability of Earth's energy budget as simulated  
19 by CMIP5 climate models, *Env. Res. Lett.*, 9 (3), 2014.
- 20 Pardaens A. K., Banks, H. T., Gregory, J. M. and Rowntree, P. R.: Freshwater transports in  
21 HadCM3, *Climate Dynamics*, 21, 177-195, 2003.
- 22 Pradal, M.-A., and Gnanadesikan, A.: How Does the Redi Parameter for Mesoscale Mixing  
23 Impact Global Climate in an Earth System Model? *Journal of Advances in Modeling the*  
24 *Earth System*, 6:586-601, 2014.
- 25 Rae, J. G. L., Hewitt, H. T., Keen, A. B., Ridley, J. K., West, A. E., Harris, C. M., Hunke, E.  
26 C. and Walters, D. N.: Development of Global Sea Ice 6.0 CICE configuration for the Met  
27 Office Global Coupled Model, *Geosci. Model Dev.*, 8, 2221-2230, doi:10.5194/gmd-8-2221-  
28 2015, 2015.



- 1 Sanchez-Gomez, E., Cassou, C., Ruprich-Robert, Y., Fernandez, E., and Teray, L.: Drift  
2 dynamics in a coupled model initialized for decadal forecasts, doi :10.1007/s00382-015-2678-  
3 y, *Clim. Dyn.*, 46, 1819–1840, 2016.
- 4 Sheldon, L., and Czaja, A.: Seasonal and interannual variability of an index of deep  
5 atmospheric convection over western boundary currents. *Q J R Meteorol Soc* 140: 22–30. doi:  
6 10.1002/qj.2103, 2014.
- 7 Small, R. J., Bacmeister, J., Bailey, D. A., Baker, A., Bishop, S., Bryan, F. O., Caron, J.,  
8 Dennis, J., Gent, P. R., Hsu, H.-M., Jochum, M., Lawrence, D. M., Munoz Acevedo, E.,  
9 diNezio, P., Scheitlin, T., Tomas, R., Tribbia, J., Tseng, Y. and Vertenstein, M.: A new  
10 synoptic-scale resolving global climate simulation using the Community Earth System Model.  
11 *Journal of Advances in Modeling Earth Systems*, 6, 1065-1094, DOI:  
12 10.1002/2014MS000363, 2014.
- 13 Tréguier, A.-M., Deshayes, J., Lique, C., Dussin, R. and Molines, J.-M.: Eddy contributions  
14 to the meridional transport of salt in the North Atlantic. *Journal of Geophysical Research.*  
15 *Oceans*, Wiley-Blackwell, 117, doi:10.1029/2012JC007927, 2012.
- 16 Valcke, S., Craig, T. and Coquart, L.: OASIS3-MCT User Guide, OASIS3-MCT 3.0,  
17 Technical Report, TR/CMGC/15/38, CERFACS/CNRS SUC URA No 1875, Toulouse,  
18 France, 2015.
- 19 Vellinga, M. and Wu, P.: Low-Latitude Freshwater Influence on Centennial Variability of the  
20 Atlantic Thermohaline Circulation. *J. Climate*, 17, 4498–4511, doi: 10.1175/3219.1, 2004.
- 21 Williams, K. D., Harris, C. M., Bodas-Salcedo, A., Camp, J., Comer, R. E., Copsey, D.,  
22 Fereday, D., Graham, T., Hill, R., Hinton, T., Hyder, P., Ineson, S., Masato, G., Milton, S. F.,  
23 Roberts, M. J., Rowell, D. P., Sanchez, C., Shelly, A., Sinha, B., Walters, D. N., West, A.,  
24 Woollings, T. and Xavier, P. K.: The Met Office Global Coupled model 2.0 (GC2)  
25 configuration. *Geosci. Model Dev.*, 8, 1509-1524, doi:10.5194/gmd-8-1509-2015, 2015.
- 26 Zhang Y. and Vallis, G. K.: Ocean Heat Uptake in Eddying and Non-Eddying Ocean  
27 Circulation Models in a Warming Climate, *J. Phys. Oceanogr.*, 43 (10), 2211-2229,  
28 doi:10.1175/JPO-D-12-078.1, 2013.
- 29



1 Table 1. Coupled models used in this paper

Model	Horizontal Resolution	Coupling frequency
GC2 (Williams et al., 2015)	N216-ORCA025	3-hourly
GC2-N512	N512-ORCA025	3-hourly
GC2.1 (this paper)	N216-ORCA025	1-hourly
GC2.1-N512O12	N512-ORCA12	1-hourly

2

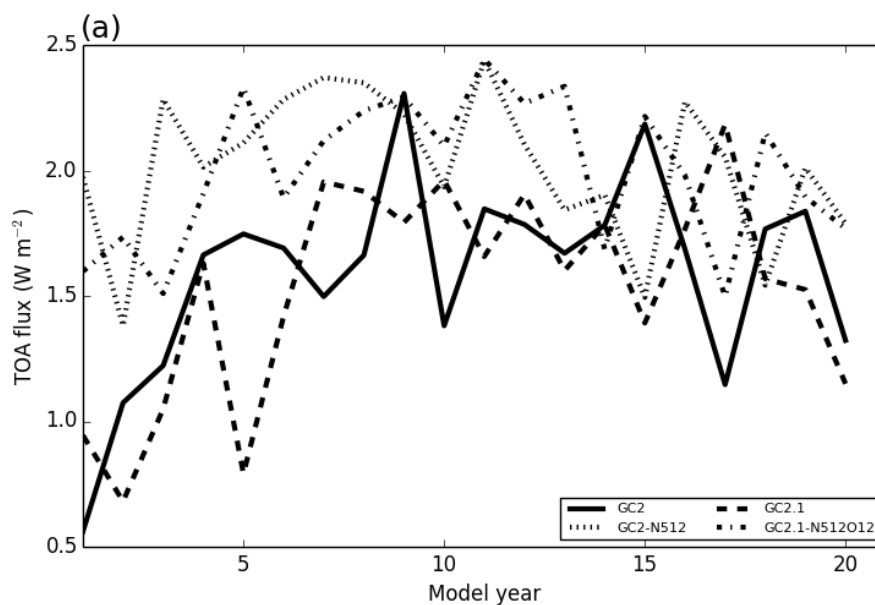
3

4 Table 2. Key metrics from years 11-20 of the experiments and observations. TOA  
 5 observations from CERES/EBAF for years 2000-2010. Global mean SST error (compared to  
 6 Reynolds OI). Overflows are calculated as southward flow across the Greenland-Iceland-  
 7 Scotland ridge below density of  $27.8 \text{ kg m}^{-3}$  and have standard deviation shown in brackets.

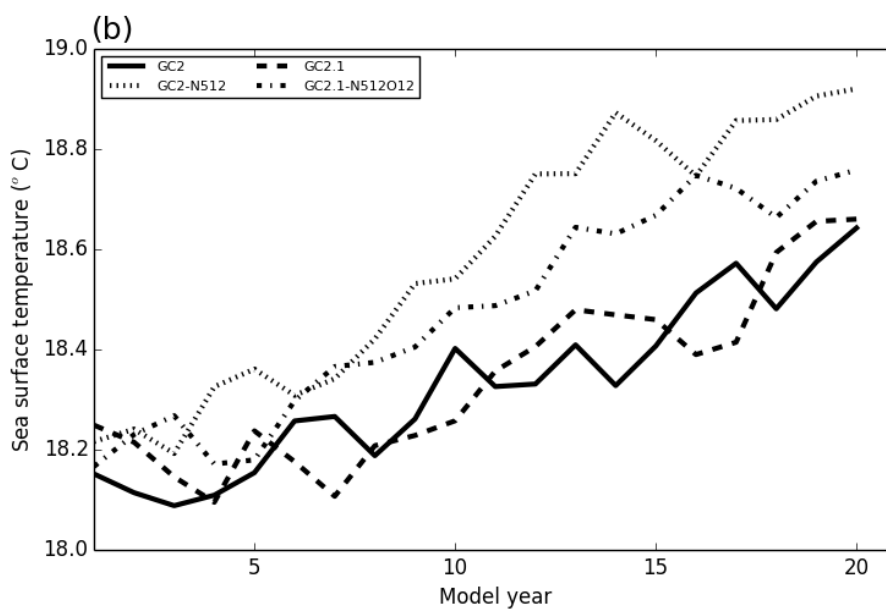
Model	Net TOA ( $\text{W/m}^2$ )	Global mean SST error (K)	Maximum overturning at 30°S (Sv)	Maximum overturning at 24°N (Sv)	Net transport from overflows (Sv)
Observations	0.85				
GC2	1.61	0.25	13.7	14.6	4.0 (0.24)
GC2-N512	1.79	0.60	14.3	14.9	3.9 (0.28)
GC2.1	1.64	0.29	14.3	16.4	4.7 (0.26)
GC2.1- N512O12	2.02	0.44	17.5	17.7	5.9 (0.42)

8





1  
2

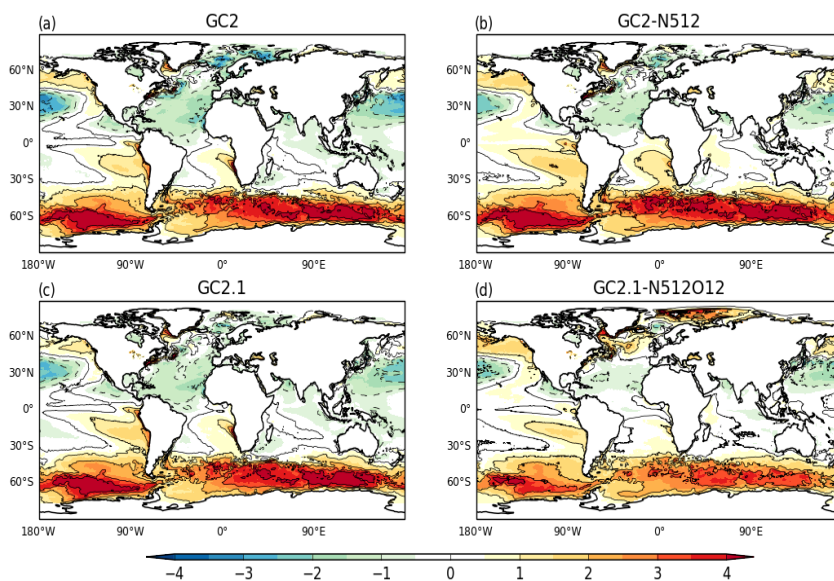


3  
4

5 Figure 1: Timeseries of a) net TOA and b) global mean SST from GC2, GC2-N512, GC2.1  
6 and GC2.1-N512O12.



1



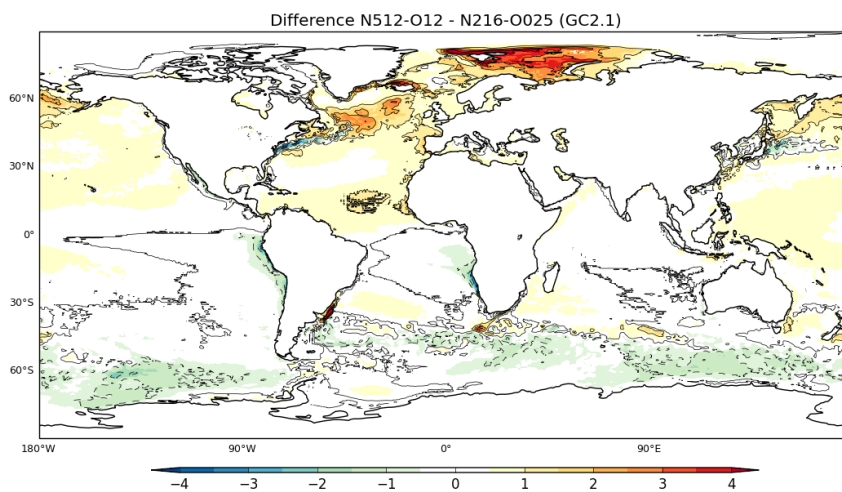
2

3

4 Figure 2: Differences between modelled SST from years 11-20 and observed SST from  
5 HadISST (°C) for a) GC2, b) GC2-N512, c) GC2.1 and d) GC2.1-N512012.

6

7

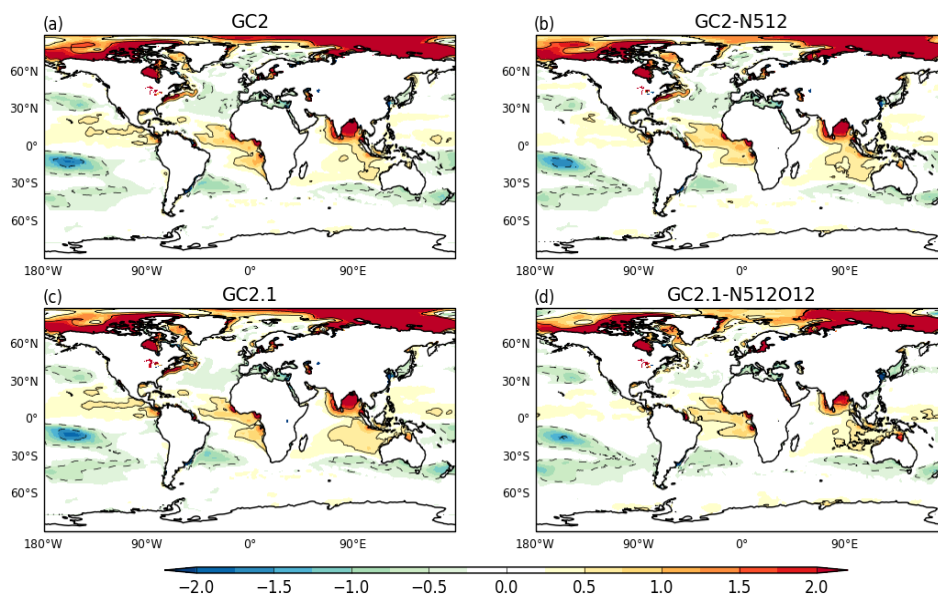


1  
2  
3

Figure 3: SST difference (°C) for years 11-20 between GC2.1-N512O12 and GC2.1



1



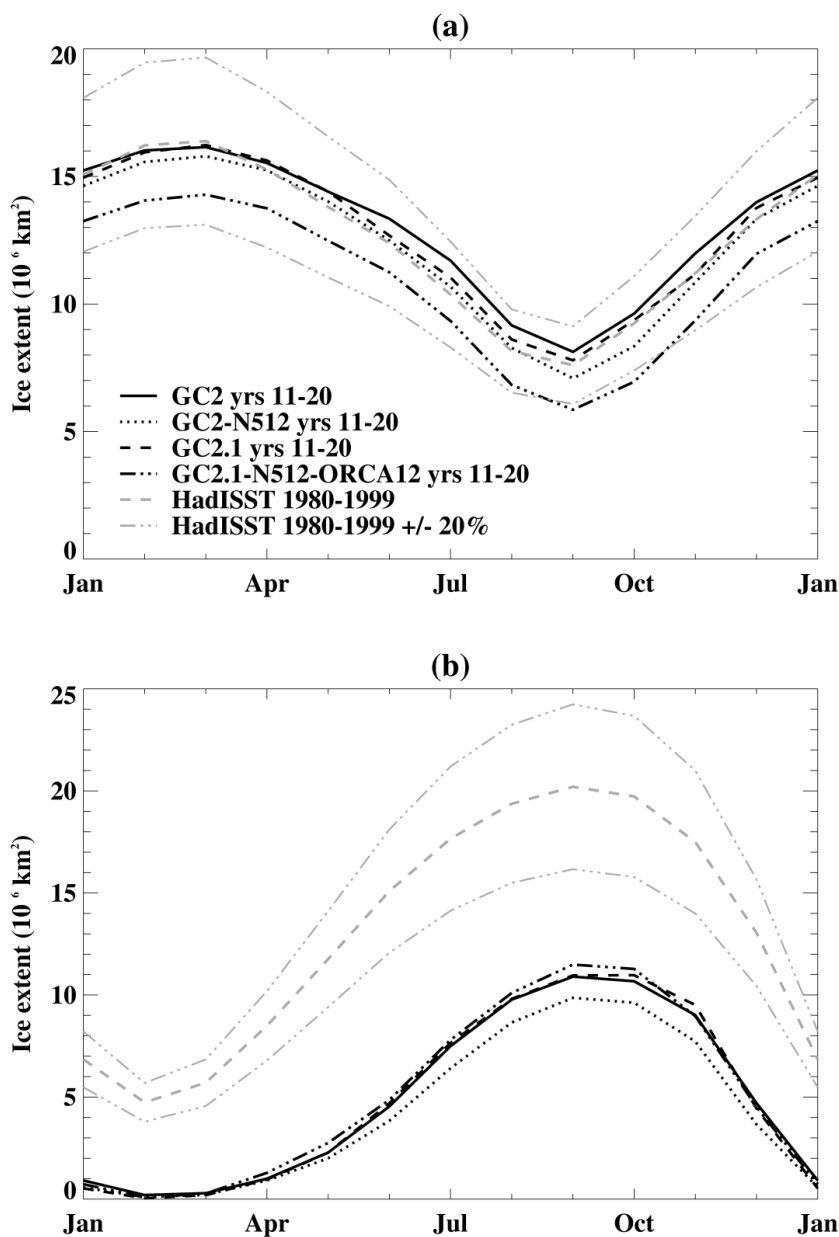
2  
3

4 Figure 4: Differences between modelled SSS from years 11-20 and observed SSS from EN4  
5 (psu) for a) GC2, b) GC2-N512, c) GC2.1 and d) GC2.1-N512O12.

6



1

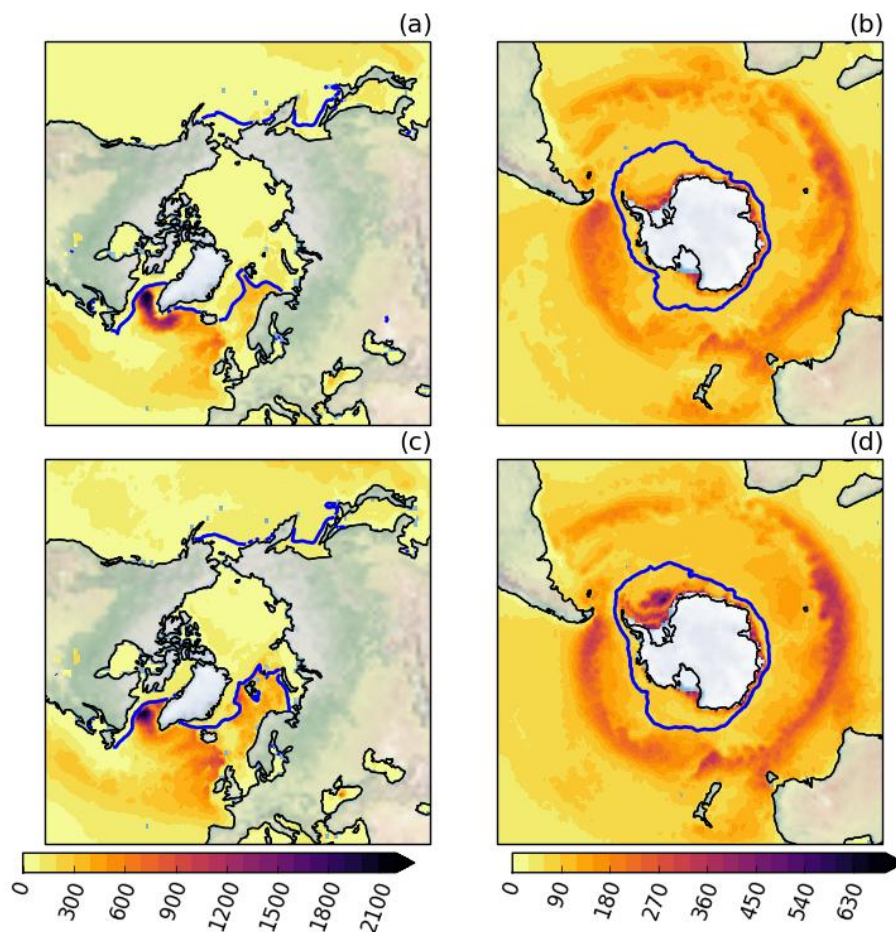


2  
3  
4  
5  
6

Figure 5: Seasonal cycle of sea ice extent in a) Northern and b) Southern hemisphere for years 11-20 compared against HadISST 1980-99 and with  $\pm 20\%$  error bars denoted.

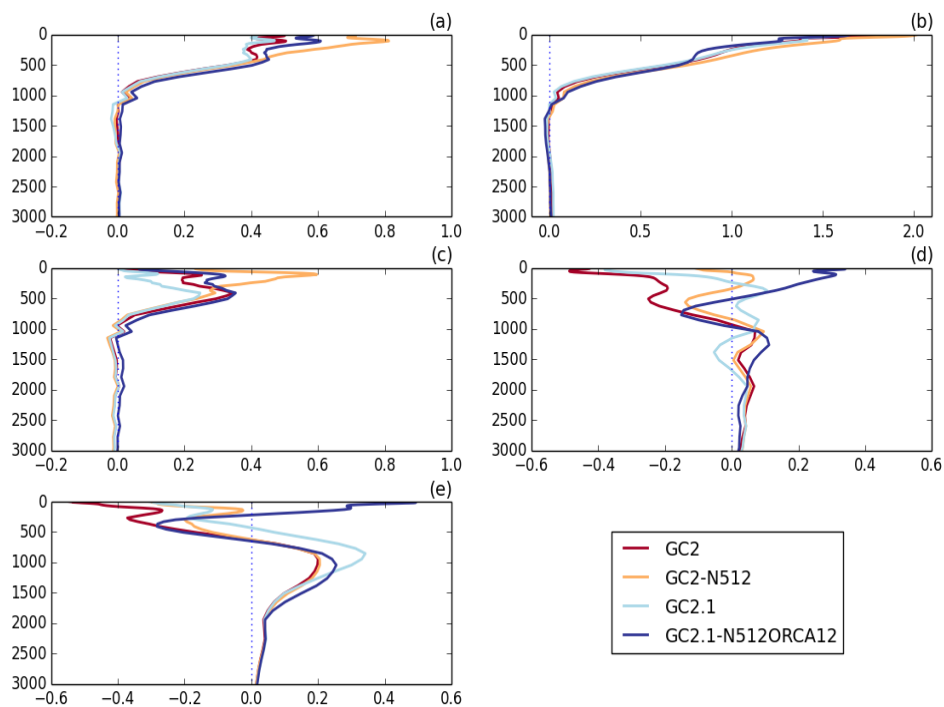


1



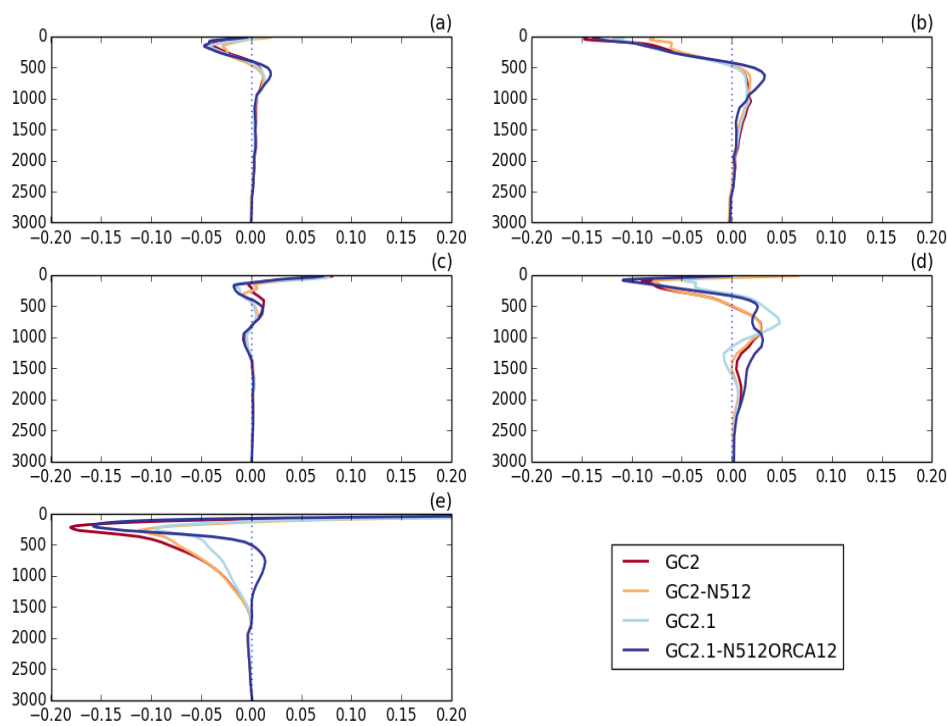
2  
3  
4  
5  
6  
7  
8

Figure 6: Mean March Northern hemisphere winter mixed layer depth (m) and Arctic sea ice edge and mean September Southern hemisphere winter mixed layer depth (m) and sea ice edge for years 11-20 for GC2 (a,b) and GC2.1-N512O12 (c,d)



1  
2  
3  
4  
5  
6  
7  
8

Figure 7: Area-weighted mean temperature difference (years 11-20 minus year 1; °C) for GC2, GC2-N512, GC2.1 and GC2.1-N512O12 for a) global, b) 90S-30S, c) 30S-30N, d) 30N-90N, e) 65N-90N. Note the range on the x-axis is equal in all panels except (b). The vertical axis denotes depth (m).



1

2 Figure 8: Area-weighted mean salinity difference (years 11-20 minus year 1; psu) for GC2,  
3 GC2-N512, GC2.1 and GC2.1-N512ORCA12 for a) global, b) 90S-30S, c) 30S-30N, d) 30N-90N,  
4 e) 65N-90N. The vertical axis denotes depth (m).

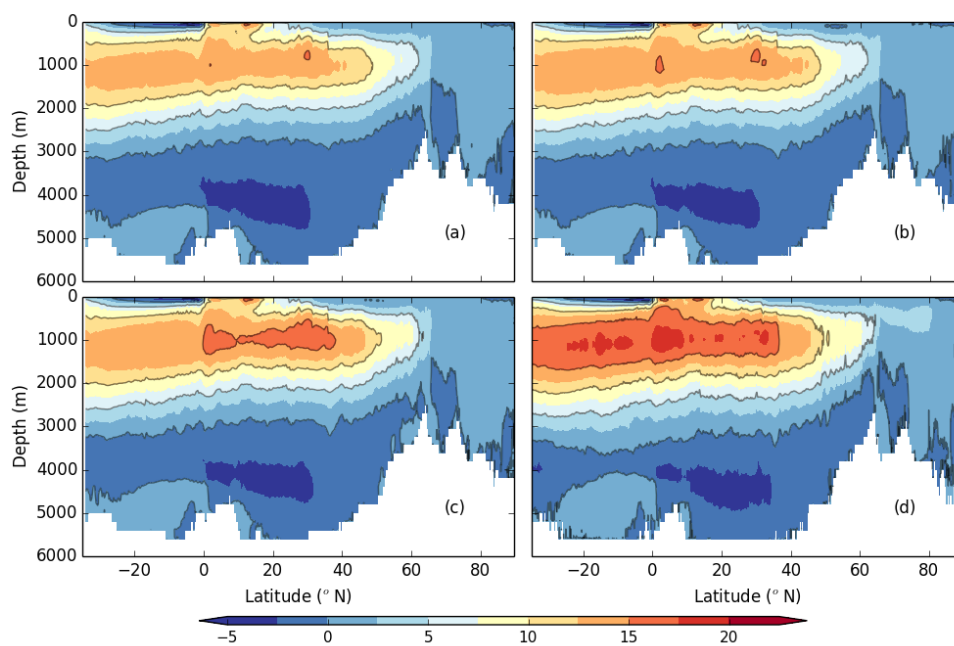
5

6





1



2

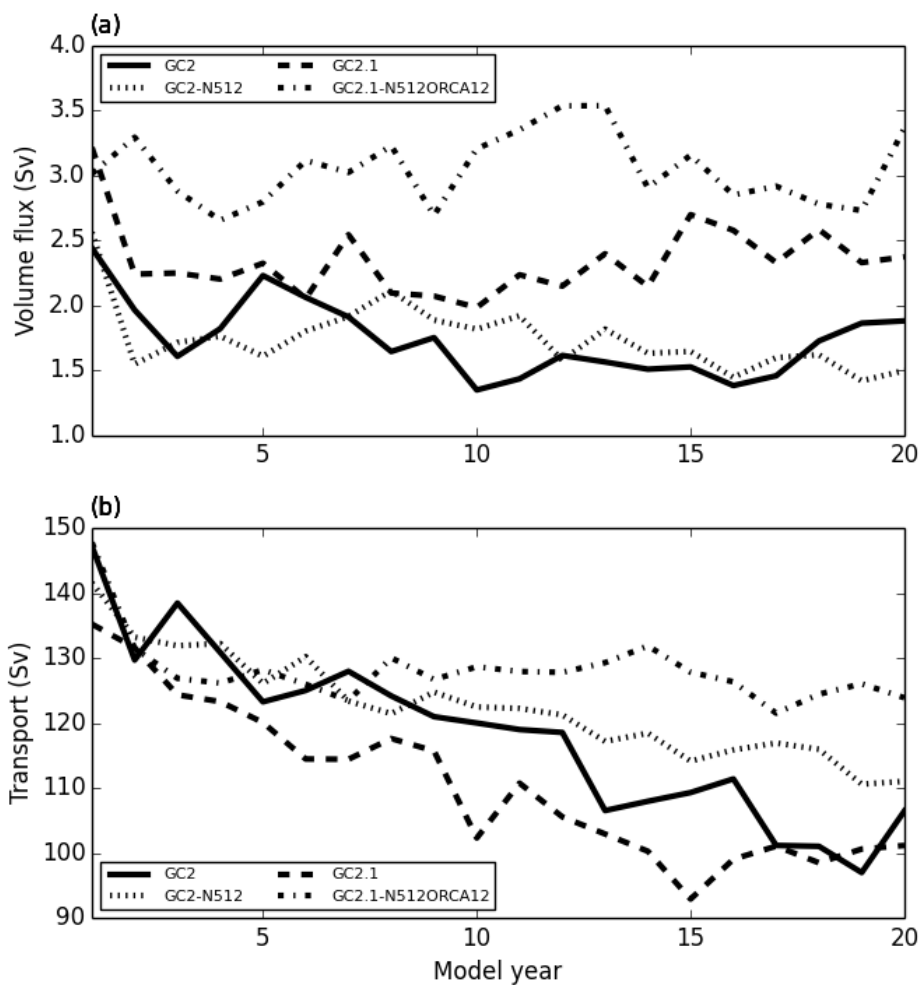
3

4 Figure 9: Atlantic Meridional overturning for (a) GC2, (b) GC2-N512, (c) GC2.1 and (d)  
5 GC2.1-N512O12, meaned over years 11-20. Contours in Sverdrups ( $10^6 \text{ m}^3 \text{ s}^{-1}$ ), with line  
6 contour spacing of 5 Sv.

7



1

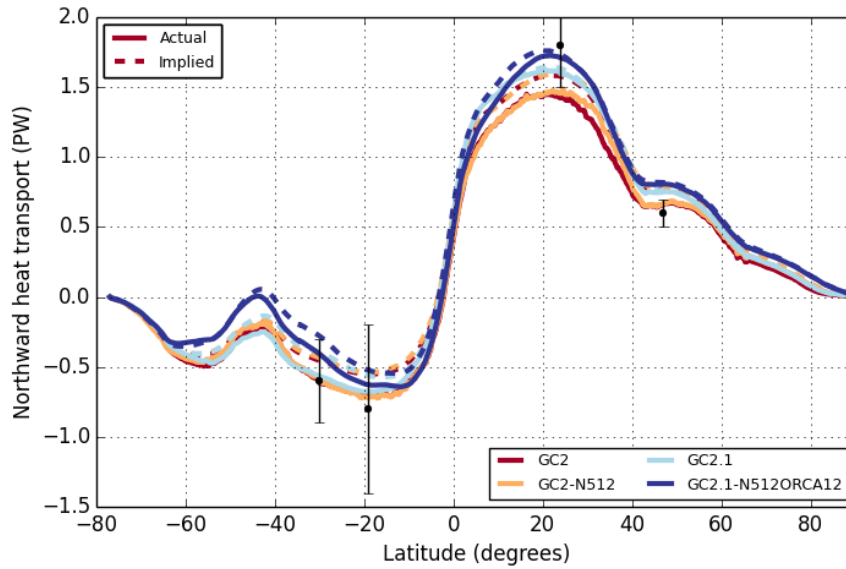


2

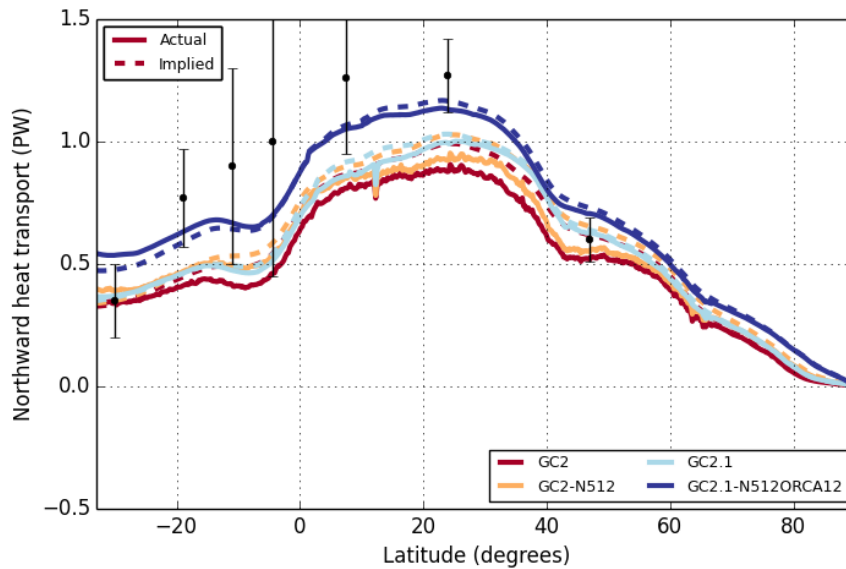
3

4 Figure 10: a) Denmark Straits volume flux (Sv) (calculated as southward flow across the  
5 Greenland-Iceland-Scotland ridge below density of  $27.8 \text{ kg m}^{-3}$ ) and b) Antarctic Circumpolar  
6 Current transport (Sv) from GC2, GC2-N512, GC2.1 and GC2.1-N512O12

7



1



2  
3

4 Figure 11: Actual (bold) and implied (dashed) northward heat transports from GC2, GC2-  
5 N512, GC2.1 and GC2.1-N512O12 for (a) global and (b) Atlantic basins. The implied  
6 transport (integrated southwards from the pole using the ocean surface heat flux) uses heat  
7 fluxes in which the global mean imbalance has been removed at every point. Observational  
8 estimates and associated error bars from Ganachaud and Wunsch (2003) are shown.